Catalysis Letters, Vol. 115, Nos. 3–4, June 2007 (© 2007)
DOI: 10.1007/s10562-007-9119-4

MgO-supported cluster catalysts with Pt–Ru interactions prepared from $Pt_3Ru_6(CO)_{21}(\mu_3\text{-H})(\mu\text{-H})_3$

Saowapa Chotisuwan,[a,b,c] Jatuporn Wittayakun,[b] Rodrigo J. Lobo-Lapidus,[a] and Bruce C. Gates[a,*]

[a]*Department of Chemical Engineering and Materials Science, University of California, Davis, CA, USA*
[b]*School of Chemistry, Suranaree University of Technology, Nakhon Ratchasima, Thailand*
[c]*Department of Science, Prince of Songkla University, Pattani, Thailand*

Received 4 April 2007; accepted 4 April 2007

Bimetallic MgO-supported catalysts were prepared by adsorption of $Pt_3Ru_6(CO)_{21}(\mu_3\text{-H})(\mu\text{-H})_3$ on porous MgO. Characterization of the supported clusters by infrared (IR) spectroscopy showed that the adsorbed species were still in the form of metal carbonyls. The supported clusters were decarbonylated by treatment in flowing helium at 300 °C, as shown by IR and extended X-ray absorption fine structure (EXAFS) data, and the resulting supported PtRu clusters were shown by EXAFS spectroscopy to have metal frames that retained Pt–Ru bonds but were slightly restructured relative to those of the precursor; the average cluster size was almost unchanged as a result of the decarbonylation. These are among the smallest reported bimetallic clusters of group-8 metals. The decarbonylated sample catalyzed ethylene hydrogenation with an activity similar to that reported previously for γ-Al_2O_3-supported clusters prepared in nearly the same way and having nearly the same structure. Both samples were also active for *n*-butane hydrogenolysis, with the MgO-supported catalyst being more active than the γ-Al_2O_3-supported catalyst.

KEY WORDS: bimetallic catalyst; PtRu clusters; magnesia; MgO; ethylene hydrogenation; *n*-butane hydrogenolysis; EXAFS spectroscopy.

1. Introduction

Supported bimetallic particles containing platinum are important industrial catalysts. Examples include Pt–Ir on alumina and Pt–Re on alumina, which have been applied in naphtha reforming [1]. Supported bimetallic catalysts with high metal dispersions offer structures and catalytic properties different from those of bimetallic catalysts with low dispersions and bulk-like properties [1], and there are excellent opportunities for preparing highly dispersed bimetallic catalysts with new properties.

An effective method for preparation of bimetallic cluster catalysts in which the two metals are bonded to each other involves adsorption of a molecular bimetallic carbonyl cluster precursor on a support. Typically, such preparations lead to supported catalysts with structures that are markedly different from those of the metal frames of the precursors, because fragmentation and/or aggregation of the metal take place during treatments that remove the carbonyl ligands. In some cases, however, the carbonyl ligands have been removed from the metal frames of supported clusters without substantial changes in the frame [2], but there are few such examples for bimetallic catalysts consisting of group-8 metals, because these readily undergo aggregation under the conditions required for decarbonylation [2,3].

For example, a catalyst was prepared from $Pt_3Ru_6(CO)_{21}(\mu_3\text{-H})(\mu\text{-H})_3$ on γ-Al_2O_3, which was decarbonylated in flowing helium 300 °C [4]; EXAFS data indicate that the metal carbonyl remained intact upon adsorption on the support, undergoing only slight changes in the structure of the metal frame. After decarbonylation, the bonds between the metals and support oxygen atoms became stronger, and the number of Pt–Ru bonds per cluster decreased to approximately half that of the precursor, but the resultant supported clusters were still similar in size to the metal frame of the precursor.

The success of such a preparation depends on the relative strengths of the metal–metal and metal–support bonds, and thus the choice of the support is important. Our goal in this work was to investigate the role of a support that is more basic than γ-Al_2O_3, namely, MgO, in the preparation of supported catalysts from $Pt_3Ru_6(CO)_{21}(\mu_3\text{-H})(\mu\text{-H})_3$.

Although there are only a few reports of MgO-supported bimetallic catalysts incorporating just group-8 metals, there are a number of examples of MgO-supported catalysts incorporating platinum with an oxophilic metal, including, Pt–Sn/MgO prepared from $Pt(acac)_2$ and $Sn(n\text{-}C_4H_9)_4$ by a two-step impregnation

*To whom correspondence should be addressed.
E-mail: bcgates@ucdavis.edu

[5], and PtW/MgO [6] and PtMo/MgO [7], prepared by slurrying MgO powder with pentane solutions of $\{Pt[W(CO)_3(C_5H_5)]_2(PhCN)_2\}$ and $\{Pt[Mo(CO)_3(C_5H_5)]_2(PhCN)_2\}$, respectively. The characterizations of these samples show that the oxophilic metal helps to maintain and stabilize high dispersions of the platinum [8].

We now report data representing a catalyst prepared from $Pt_3Ru_6(CO)_{21}(\mu_3\text{-}H)(\mu\text{-}H)_3$ on MgO, before and after decarbonylation, to characterize the metal–metal and metal–support bonding. The catalyst was tested for a simple structure-insensitive reaction, ethylene hydrogenation, and the structure-sensitive *n*-butane hydrogenolysis.

2. Experimental

2.1. Materials

MgO powder (EM Science, 97%, surface area approximately 70 m^2/g) was calcined in flowing O_2 at 400 °C for 2 h and evacuated (pressure $\approx 1.33 \times 10^{-3}$ mbar) for 14 h before use. Reagents used in the synthesis and purification of the cluster precursor and the reagents for catalytic testing and pretreatments are the same as those already described [4].

2.2. Sample preparation and handling

The synthesis, purification, and characterization of $Pt_3Ru_6(CO)_{21}(\mu_3\text{-}H)(\mu\text{-}H)_3$ are reported elsewhere [4]. PtRu/MgO catalysts containing 1.0 wt% Pt and 1.0 wt% Ru were prepared by slurrying MgO with $Pt_3Ru_6(CO)_{21}(\mu_3\text{-}H)(\mu\text{-}H)_3$ in CH_2Cl_2 for 1 day. After removal of the solvent by evacuation for an additional day, the sample was characterized by IR spectroscopy; the sample was then heated in flowing helium at 300 °C and atmospheric pressure for 2 h to remove ligands and characterized again by IR and EXAFS spectroscopies.

2.3. Attempted Extraction of adsorbed species

In a separate experiment, the dried supported sample was brought in contact with liquid CH_2Cl_2 at room temperature for 30 min with stirring in an attempt to extract weakly bonded species. Both the supernatant solution and the solid were characterized by IR spectroscopy.

2.4. Characterization of samples before and after decarbonylation

The MgO-supported samples prepared from $Pt_3Ru_6(CO)_{21}(\mu_3\text{-}H)(\mu\text{-}H)_3$ were characterized by IR and EXAFS spectroscopies. Because the procedures are essentially the same as those used for $\gamma\text{-}Al_2O_3$-supported samples prepared with the same precursor [4], details are omitted here.

EXAFS experiments were performed at X-ray beamline X-18B at the National Synchrotron Light Source (NSLS), Brookhaven National Laboratory (BNL), New York, USA. The storage ring energy was 2.5 GeV, and the ring current was in the range 110–250 mA. The samples were scanned at the Pt L_{III} edge (11,564 eV) and the Ru K edge (22,117 eV) in transmission mode with integration for 1 s at each energy in the range from 200 eV below the absorption edge to 975 eV beyond the edge.

2.5. Catalytic activity of supported clusters for ethylene hydrogenation

The PtRu/MgO sample was tested as an ethylene hydrogenation catalyst in a stainless-steel U-tube once-through flow reactor at atmospheric pressure. The pretreatment of the catalyst and the testing procedure were as reported elsewhere [4]. The mixture of H_2 and C_2H_4 in He flowed into reactor at a rate of 200 mL (NTP)/min. The effluent gas mixture was analyzed with an online gas chromatograph, as before [4]. The feed partial pressures of the reactants were $P_{H_2} = 107$ mbar and $P_{C_2H_4} = 53$ mbar; the temperature varied from −75 to −20 °C.

2.6. Catalytic activity of PtRu/MgO for n-butane hydrogenolysis

The PtRu/MgO was tested in a quartz once-through tubular flow reactor at atmospheric pressure. The catalyst pretreatment and testing procedures were as reported [4]. The feed to the reactor was a gas mixture containing H_2 and $n\text{-}C_4H_{10}$ in He with a flow rate of 100 mL (NTP)/min. The effluent gas mixture was analyzed with an online gas chromatograph, as before [4]. The feed partial pressures of the reactants were $P_{H_2} = 720$ mbar, $P_{n-C_4H_{10}} = 80$ mbar; the temperature was held constant in the range of 200–260 °C.

3. EXAFS data analysis

EXAFS data were analyzed with theoretical reference files calculated with the software code FEFF7.0 [9]. The EXAFS data processing was carried out with the software XDAP [10]. The final normalized EXAFS function for each edge of each sample was obtained from the average of four scans. Analysis of the EXAFS data was carried out with a difference file technique [11] and the software XDAP [10]. Because the phase shift and backscattering amplitude are to a good approximation transferable between next-near neighbors in the periodic table, the Ir–$O_{support}$, Ir–C, and Ir–O* (O* is carbonyl oxygen) phase shifts and backscattering amplitudes extracted from EXAFS data characterizing crystalline IrO_2 and $Ir_6(CO)_{16}$ were used to analyze the Pt–$O_{support}$ and Pt–CO (Pt–C and Pt–O*) interactions [12]. The

Pt–Pt, Pt–Ru, and Ru–Pt interactions were calculated from crystallographic data reported for metallic platinum [13] and $[PtRu_2(CO)_8(dppe)]$ (dppe is 1,2-bis (diphenylphosphino)ethane) [14]. As there are hydride ligands on the ruthenium in the precursor $Pt_3Ru_6(CO)_{21}(\mu_3\text{-H})(\mu\text{-H})_3$, the Ru–Ru interaction for the reference was calculated from crystallographic data characterizing a compound with such ligands, $Pt_3Ru_6(CO)_{21}(\mu_3\text{-H})(\mu\text{-H})_3$ [15]. The reference Pt–Mg interaction was generated from crystallographic data characterizing $MgPt_3$ [16].

The fitting ranges in both momentum and real space were determined by the data quality, which was very good; thus, values of k (the photoelectron wave vector) up to 15 $Å^{-1}$ were used at each metal edge. Iterative fitting was carried out until optimal agreement was attained between the calculated k^1-, k^2-, and k^3-weighted data and the postulated model (combination of absorber–backscatterer pairs). For each model, the data at each metal edge were fitted independently. For internal consistency of the fits, the bond distances and Debye–Waller factors representing the Pt–Ru interactions must be the same in the fits determined at each metal edge, and this constraint was applied in the analysis; a further constraint applied in the fitting is that $N_{Pt\text{-}Ru}/N_{Ru\text{-}Pt} = n_{Ru}/n_{Pt}$, where N is the coordination number and n_{Ru} and n_{Pt} are the total numbers of Ru and Pt atoms in the sample, respectively [1,17].

The Pt L_{III}-edge and Ru K edge EXAFS data characterizing the supported clusters were Fourier-transformed over the ranges $2.85 < k < 15.05$ $Å^{-1}$, $1.0 < r < 4.0$ Å; and $2.60 < k < 15.52$ $Å^{-1}$, $1.0 < r < 4.0$ Å, respectively (where r is the absorber–backscatterer distance). The statistically justified number of free parameters estimated from the Nyquist theorem at the Pt L_{III} and Ru K edges were 31, and 34, respectively, and the maximum number of free parameters used in any of the fits was 16, indicating that each model is justified statistically by the criterion of the Nyquist theorem [18].

4. Results

4.1. IR spectrum of metal carbonyls formed initially from $Pt_3Ru_6(CO)_{21}(\mu_3\text{-H})(\mu\text{-H})_3$ on MgO

The IR spectrum of the sample formed by adsorption of $Pt_3Ru_6(CO)_{21}(\mu_3\text{-H})(\mu\text{-H})_3$ on MgO (figure 1, spectrum C) includes broad peaks in the ν_{CO} range indicating that carbonyl ligands were present. A comparison with the spectrum of $Pt_3Ru_6(CO)_{21}(\mu_3\text{-H})(\mu\text{-H})_3$ in CH_2Cl_2 solution shows a marked broadening of the ν_{CO} peaks and a shift of each to lower wavenumbers. The peak broadening is consistent with the presence of clusters in various configurations on the nonuniform surface of the support. The absorption centered at about 2023 cm^{-1} is typical of terminal CO ligands bonded to transition metals [19] (as

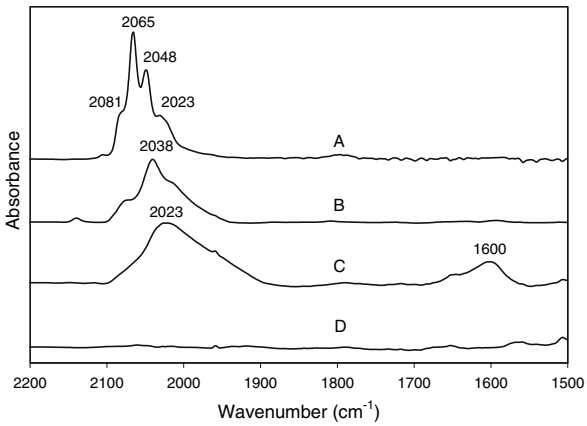

Figure 1. IR spectra in ν_{CO} region of (A) the precursor $Pt_3Ru_6(CO)_{21}(\mu_3\text{-H})(\mu\text{-H})_3$ in CH_2Cl_2; (B) dry supported sample prepared from adsorption of the precursor onto $\gamma\text{-}Al_2O_3$ [4]; (C) dry supported sample prepared from adsorption of the precursor onto MgO; (D) sample referred to in (C) after decarbonylation at 300 °C in flowing helium for 2 h. The spectra are normalized and do not allow quantitative comparisons with each other.

in $Pt_3Ru_6(CO)_{21}(\mu_3\text{-H})(\mu\text{-H})_3$). The spectrum of the supported species is not sufficient to determine the structure, but it is consistent with the presence of $Pt_3Ru_6(CO)_{21}(\mu_3\text{-H})(\mu\text{-H})_3$ on the support, with the peaks merged because of the surface nonuniformity.

The band at 1600(m) cm^{-1} (figure 1, spectrum C) is assigned to carbonates or carboxylates on the MgO surface, as these occur in the range 1700–1200 cm^{-1} [20]. These peaks are inferred not to have arisen from adventitious CO_2, because the samples were handled in the absence of air. Thus, the presence of this band suggests some partial decarbonylation of the precursor.

Numerous investigations of the reactivity of hydrido carbonyl clusters of metals with oxide supports [21] indicate the occurrence of acid-base reactions, and the interactions may be so strong that hydrido ligands are abstracted from the metal by strongly basic surface sites, as on MgO. The resultant carbonylate anions have been inferred to interact with Mg^{2+} sites through oxygen atoms of carbonyl ligands (namely, $M\text{–}CO\cdots\{Mg^{2+}\}$, where the braces denote an atom that is part of the support lattice). Such an interaction causes the carbonyl band to shift to lower frequency.

The shift of the ν_{CO} bands to lower wavenumbers in the supported bimetallic clusters is consistent with the inference that the C–O bonds in the ligands bonded to the metal were weakened as a result of the adsorption. A similar, but smaller, shift was also observed for a similarly prepared sample supported on $\gamma\text{-}Al_2O_3$ (figure 1B) [4]. The greater shift in the spectrum of the MgO-supported sample relative to that of the $\gamma\text{-}Al_2O_3$-supported sample is consistent with the stronger basicity of the MgO [21] and suggests stronger bonding to the MgO.

Attempts were made to extract the MgO-supported clusters with CH_2Cl_2. However, the color of the solid

remained essentially unchanged (brown), and the extract solution remained colorless. Furthermore, the IR spectrum of the solid remained essentially unchanged from that of the initially prepared sample. These results indicate that metal carbonyl was strongly adsorbed on the MgO. In the comparable experiment with the γ-Al_2O_3-supported sample, some extraction was observed [4], a result that confirms the suggestion that the clusters were more strongly adsorbed on MgO than on γ-Al_2O_3.

Treatment of the MgO-supported metal carbonyl in flowing helium at 300 °C for 2 h led to essentially complete removal of the carbonyl bands in the IR spectrum (figure 1, spectrum D). Thus, we infer that the decarbonylation was essentially complete, a result that was confirmed by the EXAFS data, as summarized below. The band at 1600 cm^{-1} that is suggestive of carbonates or carboxylates also disappeared as a result of this treatment.

4.2. *XANES data characterizing supported sample after decarbonylation*

The XANES data characterizing the supported sample after decarbonylation are presented in figure 2; data characterizing the γ-Al_2O_3-supported sample [4] are nearly the same. The edge energies characterizing the supported sample are also similar to those of the respective metal foils, consistent with the suggestion that the metals in the sample before and after decarbonylation were present in oxidation states near zero; the XANES data do not warrant a stronger statement.

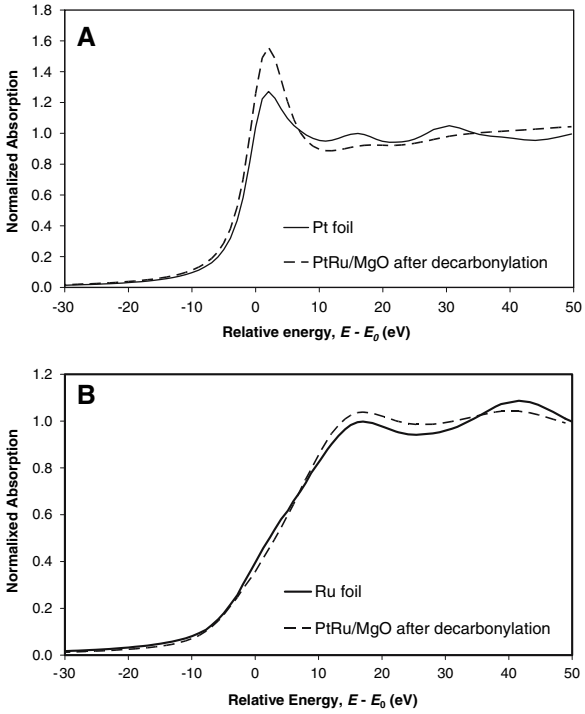

Figure 2. (A) XANES spectra scanned at the Pt L_{III} edge and (B) at the Ru K edge. The spectra are those of the MgO-supported PtRu sample prepared by adsorption of $Pt_3Ru_6(CO)_{21}(\mu_3\text{-}H)(\mu\text{-}H)_3$ and subsequent treatment in He at 300 °C, compared in (A) with the spectrum of platinum foil and in (B) with that of ruthenium foil.

4.3. *EXAFS data characterizing MgO-supported PtRu clusters after decarbonylation*

The normalized and Fourier-transformed EXAFS data characterizing the supported clusters are shown in figures 3 and 4. The data at the Pt L_{III} and Ru K edges show oscillations at k values in the range of 2.85–15.05 $Å^{-1}$ and 2.60–15.52 $Å^{-1}$, respectively. The data at high-k values indicate the presence of near-neighbor high-Z backscatterers around the Pt and Ru atoms. Furthermore, the relatively weak oscillations in the high-k region indicate the absence of large (aggregated) metal clusters in the sample.

A number of structural models were considered in the data fitting. The following absorber–backscatterer combinations were investigated:

At the Ru edge, Ru–Ru, Ru–Pt, Ru–O_s (where the subscript refers to short), Ru–O_l (where the subscript refers to long), and Ru–Mg contributions were considered in the fitting. The fitting converged to one model that was clearly superior to the others, and it includes Ru–Ru, Ru–Pt, Ru–O_s, and Ru–O_l contributions. The fit agrees very well with the data (dotted lines, figure 3). The goodness of fit was 160 and the value of $(\Delta\chi)^2$ was 209.

At the Pt edge, Pt–Pt, Pt–Ru, Pt–O_s, Pt–O_l, and Pt–Mg contributions were considered. Pt–X (where X is a light backscatterer, either O or C) contributions were also considered. Again the fitting converged to one model that was clearly superior to the others, including Pt–Pt, Pt–Ru, Pt–O_s, and Pt–O_l contributions. The goodness of fit was 180 and the value of $(\Delta\chi)^2$ was 300.

In summary, the recommended model includes four shells at each metal edge, bimetallic contributions at each metal edge, and two contributions characterizing the metal-support interface at each edge.

Difference file plots indicating the isolated metal–metal contributions (found by a difference file method) are shown in figure 3C and D for platinum and in figure 4C and D for ruthenium. These show that the fits are in good agreement with the data characterizing each of the metal–metal contributions.

The parameters determined in the fitting with the recommended model are summarized in table 1. The error bounds in these parameters are not accuracies; rather, they are precisions determined from statistical analysis of the data from the multiple scans [10]. The estimated accuracies of the EXAFS parameters (and those reported below) characterizing the metal–metal contributions are approximately as follows: coordination number N, $\pm 20\%$; distance R, $\pm 1\%$; Debye–Waller factor $\Delta\sigma^2$, $\pm 30\%$; and inner potential correction ΔE_0, $\pm 10\%$; the accuracies of the metal–oxygen contributions are somewhat less.

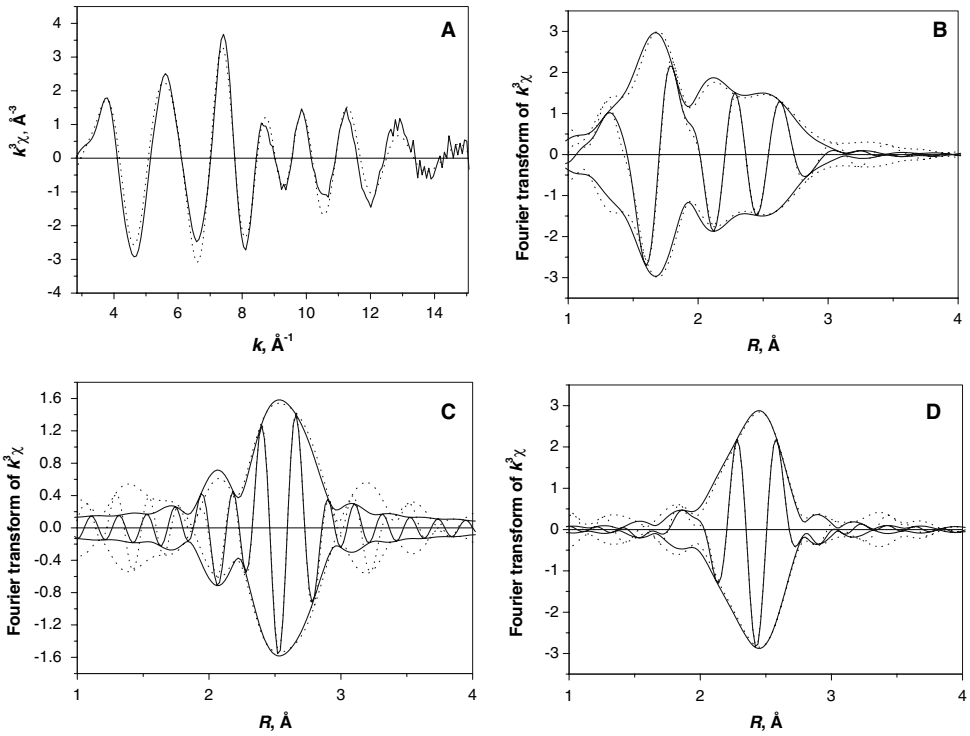

Figure 3. EXAFS data and fits: (A) Experimental k^3-weighted EXAFS ($k^3\chi$) function (solid line) and sum of the calculated contributions according to the recommended fit (dotted line). (B) Imaginary part and magnitude of uncorrected Fourier transform (k^3-weighted (Δk = 2.58–15.05 Å^{-1}) representing experimental EXAFS (solid line) and sum of the calculated contributions (dotted line)). Difference files characterizing metal–metal contributions: (C) Imaginary part and magnitude of the Fourier transform of the k^3-weighted EXAFS data (solid line) and the calculated Pt–Pt contribution (dotted line). (D) Imaginary part and magnitude of the Fourier transform of the k^3-weighted EXAFS data (solid line) and the calculated Pt–Ru contribution (dotted line).

According to this model, the data indicate Pt–Ru and Ru–Pt contributions with coordination numbers of 1.8 and 1.2, respectively. The sum of the metal–metal coordination numbers determined by the Pt edge data is 2.4, compared with a value of 6 determined by crystallographic data for the precursor $Pt_3Ru_6(CO)_{21}(\mu_3\text{-H})(\mu\text{-H})_3$ (table 1). Correspondingly, the Ru edge data indicate a value of the sum of the metal–metal coordination numbers of 4.7, compared with a value of 4 for the precursor. These data demonstrate that the supported clusters, after decarbonylation, are different in structure from the frame of the precursor and at least approximately the same size, on average.

In the fitting, two M–O contributions were identified (M = Pt, Ru); the shorter one, M–O_s, is characterized by a distance that is typical of M–O bonds and also typical of bonding of group-8 metals to oxide supports [13]. The longer M–O contribution, M–O_l, is characterized by a distance longer than a bonding distance (2.1–2.2 Å) [13]. These longer metal–oxygen distances have been observed frequently for supported group-8 metal clusters [13].

4.4. Ethylene hydrogenation catalysis

In the ethylene hydrogenation catalysis experiments, the only observed product was ethane. The conversions of ethane and H_2 fluctuated around 0.30% in the first 50 min time on stream (TOS) at a temperature of −75 °C and then became nearly constant at 0.20% for the duration of the test (up to 280 min TOS). The catalytic activities in terms of turnover frequency (TOF) and the temperature dependence of TOF (indicating the apparent activation energy, E_{app}) are shown in table 2 for our PtRu catalyst and a similarly prepared PtRu catalyst supported on γ-Al_2O_3 [4]. TOF was calculated on the basis of the inference from the EXAFS data that essentially all the metal atoms in the clusters were accessible to reactants. (The calculation ignores any lack of accessibility of Pt or Ru atoms resulting from their nearness to the support.) The rate data are summarized in the Arrhenius plots of figure 5; the rate data determine an apparent activation energy of 32 ± 3 kJ/mol.

4.5. n-Butane hydrogenolysis

The products of the reaction of *n*-butane and H_2 were methane, ethane, and propane, indicative of hydrogenolysis of the *n*-butane; furthermore, traces of *iso*-butane were also detected, indicating some isomerization. Conversions of *n*-butane were determined by adding the conversions to each of the products. At 200 °C, the conversion after about 1 min TOS was 9%; the conversion declined to 6% within 20 min TOS, becoming

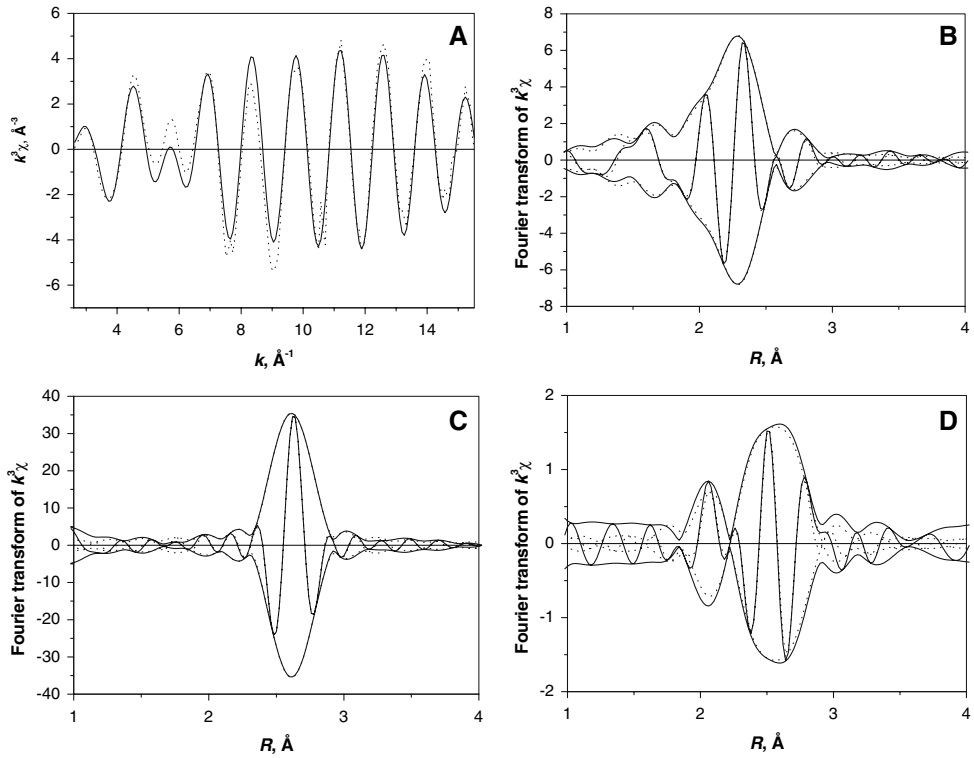

Figure 4. EXAFS data and fits: (A) Experimental k^3-weighted EXAFS ($k^3\chi$) function (solid line) and sum of the calculated contributions according to the recommended fit (dotted line). (B) Imaginary part and magnitude of uncorrected Fourier transform (k^3-weighted, Δk = 2.60–15.52 Å^{-1}) representing experimental EXAFS (solid line) and sum of the calculated contributions (dotted line). Difference files characterizing metal–metal contributions: (C) Imaginary part and magnitude of the Fourier transform of the k^3-weighted EXAFS data (solid line) and the calculated Ru–Ru contribution (dotted line). (D) Imaginary part and magnitude of the Fourier transform of the k^3-weighted EXAFS data (solid line) and the calculated Ru–Pt contribution (dotted line).

almost constant; the corresponding TOF was calculated to be $(8.2 \pm 0.1) \times 10^{-4}$ s^{-1} (figure 6). Conversions increased when the temperature was raised, and the selectivities to ethane and propane decreased and that to methane increased (figure 7).

5. Discussion

5.1. Structures of the bimetallic clusters

The EXAFS results show clearly that bimetallic structures were retained after adsorption of $Pt_3Ru_6(CO)_{21}(\mu_3\text{-H})(\mu\text{-H})_3$ and decarbonylation at 300 °C. The metal–metal coordination numbers (table 1) demonstrate that the cluster frames on the support were highly resistant to aggregation. These are among the smallest supported clusters of group-8 metals with a substantial fraction of the metal–metal interactions being bimetallic [8].

A catalyst was made similarly from the same precursor on a γ-Al_2O_3 support [4]. Like the supported clusters reported here, those dispersed on γ-Al_2O_3 were characterized by significant bimetallic interactions and a structure on average that was different from that of the metal frame of the precursor and not much different in size.

A comparison of the metal–metal coordination numbers characterizing the MgO- and γ-Al_2O_3-supported samples and the precursor is shown in table 3.

The comparison shows the following: (a) for both supports, the following metal–metal contributions became smaller relative to the precursor: Pt–Pt, Pt–Ru, and Ru–Pt; on the other hand, the Ru–Ru contributions became larger (although perhaps not significantly larger for the γ-Al_2O_3-supported sample; (b) the coordination numbers characterizing the Pt–Ru contributions in the two supported catalysts are about the same; the same is true for the Ru–Pt contributions; (c) the monometallic contributions in the two supported catalysts appear to be significantly different from each other, and the changes with respect the precursor are greater for the MgO-supported sample than for the γ-Al_2O_3-supported sample.

These data at best provide a preliminary basis for suggesting structural models of the average supported bimetallic clusters [4]. We infer that in each sample the metal clusters were bonded rather strongly to the support, as indicated by the significant metal-oxygen

Table 1
Summary of structural data characterizing crystalline $Pt_3Ru_6(CO)_{21}(\mu_3\text{-H})(\mu\text{-H})_3$ [15] and samples formed from this cluster on MgO and γ-Al_2O_3 [4] after treatment in He at 300 °C for 2 h

Edge	Shell	XRD data characterizing $Pt_3Ru_6(CO)_{21}(\mu_3\text{-H})(\mu\text{-H})_3$ [15]		EXAFS data characterizing sample prepared by adsorption of $Pt_3Ru_6(CO)_{21}(\mu_3\text{-H})(\mu\text{-H})_3$ on MgO after treatment in He at 300°C for 2 h				EXAFS data characterizing sample prepared by adsorption of $Pt_3Ru_6(CO)_{21}(\mu_3\text{-H})(\mu\text{-H})_3$ on γ-Al_2O_3 after treatment in He at 300°C for 2 h [4]			
		N	R (Å)	N	R (Å)	$10^3 \times \Delta\sigma^2$ (Å^2)	ΔE_0 (eV)	N	R (Å)	$10^3 \times \Delta\sigma^2$ (Å^2)	ΔE_0 (eV)
Pt L_{III}	Pt–Pt	2.0	2.64	0.6 ± 0.0	2.66 ± 0.00	3.2 ± 0.1	9.2 ± 0.0	1.7 ± 0.2	2.64 ± 0.01	3.0 ± 0.7	−4.5 ± 0.8
	Pt–Ru	4.0	2.80	1.8 ± 0.0	2.69 ± 0.00	6.6 ± 0.1	11.0 ± 0.0	2.2 ± 0.1	2.68 ± 0.01	4.2 ± 0.5	6.0 ± 0.3
	Pt–CO										
	Pt–C	1.0	1.85	–	–	–	–	–	–	–	–
	Pt–O*	1.0	2.99	–	–	–	–	–	–	–	–
	$Pt–O_{support}$										
	$Pt–O_s$	–	–	2.3 ± 0.0	2.02 ± 0.00	5.8 ± 0.0	9.6 ± 0.0	2.2 ± 0.1	2.08 ± 0.01	11.3 ± 1.4	8.7 ± 0.6
	$Pt–O_l$	–	–	1.3 ± 0.0	2.99 ± 0.00	0.4 ± 0.2	2.9 ± 0.0	0.8 ± 0.1	2.99 ± 0.02	−2.3 ± 2.0	−7.6 ± 1.4
Ru K	Ru–Ru	2.0	2.64	3.5 ± 0.0	2.62 ± 0.00	4.7 ± 0.1	1.0 ± 0.0	2.1 ± 0.1	2.62 ± 0.01	4.1 ± 0.3	−13.3 ± 0.3
	Ru–Pt	2.0	2.80	1.2 ± 0.0	2.70 ± 0.00	5.9 ± 0.2	11.9 ± 0.1	1.0 ± 0.1	2.68 ± 0.01	4.5 ± 0.7	−11.5 ± 1.0
	Ru–CO										
	Ru–C	3.0	1.85	–	–	–	–	–	–	–	–
	Ru–O*	3.0	2.99	–	–	–	–	–	–	–	–
	$Ru–O_{support}$										
	$Ru–O_s$	–	–	1.0 ± 0.0	1.96 ± 0.00	9.0 ± 0.2	5.3 ± 0.0	1.2 ± 0.1	2.06 ± 0.01	10.9 ± 1.7	4.1 ± 0.7
	$Ru–O_l$	–	–	2.0 ± 0.0	2.62 ± 0.00	0.2 ± 0.0	7.8 ± 0.0	2.1 ± 0.1	2.89 ± 0.01	0.1 ± 0.7	11.8 ± 0.2

Notation: O* refers to carbonyl oxygen; O_s and O_l refer to support oxygen at short and long distances, respectively; N, coordination number; R, absorber–backscatterer distance; $\Delta\sigma^2$, Debye–Waller factor relative to reference; and ΔE_0, inner potential correction relative to reference.

Table 2
Catalyst performance data for ethylene hydrogenation at atmospheric pressure with the feed partial pressures of $P_{H_2} = 80$ Torr and $P_{C_2H_4} = 40$ Torr

Catalyst	TOF $\times 10^4$ (s^{-1}) at −40 °C	E_{app} (kJ/mol)	Temperature range for measurement of E_{app} (°C)	Reference
PtRu/γ-Al_2O_3	12	35	−75 to −20	[4]
PtRu/MgO	57	32	−75 to −30	This work

TOF is turnover frequency; E_{app} is apparent activation energy.

coordination numbers characterized by bonding distances near 2.0 Å.

On MgO, the clusters appear to be enriched in platinum at the edges, as indicated by the results showing Pt–O_s was greater than Ru–O_s.

5.2. Catalysis by supported bimetallic clusters

The catalyst described here and a similar catalyst prepared from the same precursor on γ-Al_2O_3 were both found to be active for ethylene hydrogenation. The activities of these catalysts are compared in table 2. The MgO-supported catalyst is about five times more active than the γ-Al_2O_3-supported catalyst, and the apparent activation energies are approximately the same. This modest effect of the support could indicate differences between MgO and γ-Al_2O_3 as ligands to the clusters [23] or differences in the morphologies of the bimetallic clusters on the two supports.

The conversion in *n*-butane hydrogenolysis on the MgO-supported catalyst was higher than that observed with the γ-Al_2O_3-supported catalyst [4] at each reaction temperature. Furthermore, the selectivity for ethylene of the MgO-supported catalyst, which decreased with temperature, was lower than that of the γ-Al_2O_3-supported catalyst.

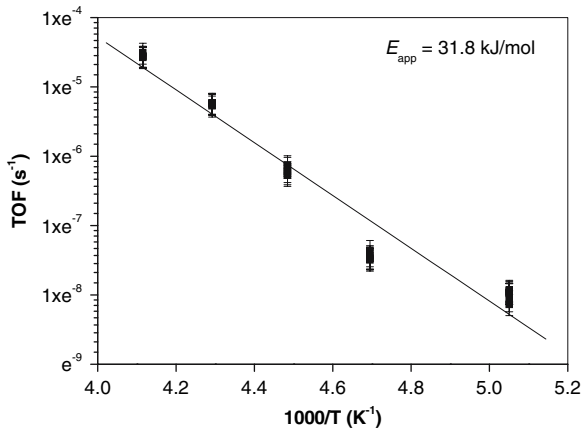

Figure 5. Arrhenius plot characterizing ethylene hydrogenation catalyzed by PtRu/MgO.

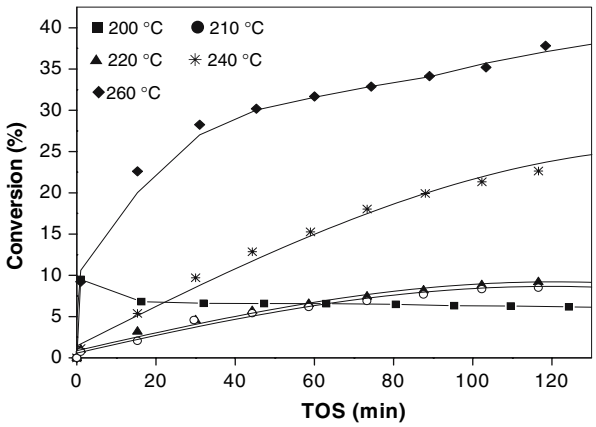

Figure 6. Dependence of catalytic activity of PtRu/MgO on time on stream (TOS) in a flow reactor for *n*-butane hydrogenolysis. The catalyst mass, feed composition, and feed flow rate are stated in the text.

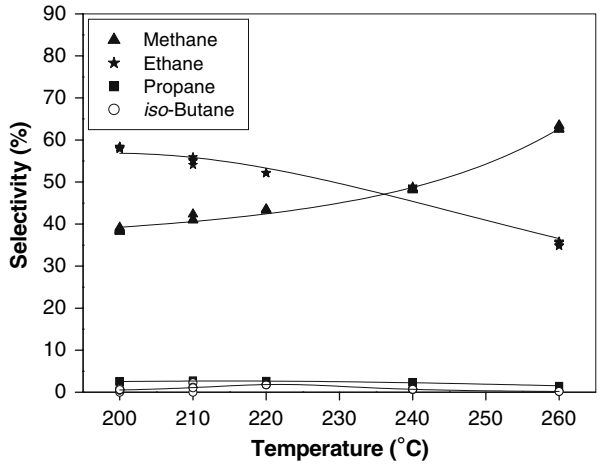

Figure 7. Dependence of selectivity on reaction temperature for *n*-butane hydrogenolysis catalyzed by PtRu/MgO. The catalyst mass, feed composition, and feed flow rate are stated in the text.

Table 3
Metal–metal coordination numbers characterizing the MgO- and γ-Al_2O_3-supported samples and the precursor $Pt_3Ru_6(CO)_{21}(\mu_3\text{-H})(\mu\text{-H})_3$

Sample	$N_{Pt\text{-}Pt}$	$N_{Ru\text{-}Ru}$	$N_{Pt\text{-}Ru}$	$N_{Ru\text{-}Pt}$	Reference
$Pt_3Ru_6(CO)_{21}(\mu_3\text{-H})(\mu\text{-H})_3$[a]	2.0	2.0	4.0	2.0	[15]
Pt–Ru clusters on MgO[b]	0.6	3.5	1.8	1.2	This work
Pt–Ru clusters on γ-Al_2O_3[b]	1.7	2.1	2.2	1.0	[4]

[a]From single-crystal X-ray diffraction.
[b]From EXAFS spectroscopy.
N is coordination number.

6. Conclusions

PtRu/MgO catalysts with Pt–Ru bonds were prepared by adsorption of $Pt_3Ru_6(CO)_{21}(\mu_3\text{-}H)(\mu\text{-}H)_3$ on MgO followed by decarbonylation in flowing helium at 300 °C. As a result of the adsorption and decarbonylation, the PtRu cluster frames underwent changes in structure without substantial changes in the average cluster size. The PtRu/MgO catalyst was found to be active for ethylene hydrogenation, with properties similar to those of the previously reported PtRu/γ-Al_2O_3 prepared from the same precursor, with a turnover frequency of $6 \times 10^{-3}\ s^{-1}$ at −40 °C with an apparent activation energy of 32 kJ/mol. The activity of PtRu/MgO for *n*-butane hydrogenolysis at 200 °C was found to be approximately five-fold greater than that of PtRu/γ-Al_2O_3 that had been prepared similarly.

Acknowledgments

We thank N. E. Schore of the University of California, Davis, for access to synthesis equipment. Financial support for S. C. was provided by the Ministry of University Affairs and Prince of Songkla University, Pattani Campus, Thailand; support was also provided by the U.S. Department of Energy, Office of Energy Research, Office of Basic Energy Sciences (Contract FG02–87ER13790). EXAFS experiments were performed at beamline X-18B at the National Synchrotron Light Source, BNL. The EXAFS data were analyzed with the software XDAP [10].

References

[1] J.H. Sinfelt, *Bimetallic Catalysts: Discoveries, Concepts, and Applications* (Wiley, New York, 1983).
[2] O. Alexeev and B.C. Gates, Ind. Eng. Chem. Res. 42 (2003) 1571.
[3] O.-B. Yang, M. Shirai, W.A. Weber and B.C. Gates, J. Phys. Chem. B 102 (1998) 8771.
[4] S. Chotisuwan, J. Wittayakun and B.C. Gates, J. Phys. Chem. B. 110 (2006) 12459.
[5] S. Recchia, C. Dossi, N. Poli, A. Fusi and L.S.R. Psaro, J. Catal. 184 (1999) 1.
[6] O. Alexeev, M. Shelef and B.C. Gates, J. Catal. 164 (1996) 1.
[7] O. Alexeev, S. Kawi, M. Shelef and B.C. Gates, J. Phys. Chem. 100 (1996) 253.
[8] O. Alexeev and B.C. Gates, Ind. Chem. Eng. Res. 42 (2003) 1571.
[9] A.L. Ankudinov and J. Rehr, Phys. Rev. B 56 (1997) R1712.
[10] M. Vaarkamp, J.C. Linders and D.C. Koningsberger, Physica B 209 (1995) 159.
[11] D.C. Koningsberger, B.L. Mojet, G.E. van Dorssen and D.E. Ramaker, Top. Catal. 10 (2000) 143.
[12] B.L. Mojet and D.C. Koningsberger, Catal. Lett. 39 (1996) 191.
[13] D.C. Koningsberger and B.C. Gates, Catal. Lett. 14 (1992) 271.
[14] R.D. Adams, G. Chen and W. Wu, J. Clust. Sci. 4 (1993) 119.
[15] R.D. Adams, T.S. Barnard, Z. Li, W. Wu and J. Yamamoto, Organometallics 13 (1994) 2357.
[16] H.H. Stadelmaier and W.K. Hardy, Z. Metallkd. 52 (1961) 391.
[17] O. Alexeev, G.W. Graham, M. Shelef, R.D. Adams and B.C. Gates, J. Phys. Chem. B 106 (2002) 4697.
[18] E.A. Stern, Phys. Rev. B 48 (1993) 9825.
[19] D.F. Shriver, H.D. Kaesz and R.D. Adams, Eds., The Chemistry of Metal Cluster Complexes (VCH, Weinheim, 1990).
[20] D.G. Rethwisch and J.A. Dumesic, Langmuir 2 (1986) 73.
[21] H.H. Lamb, B.C. Gates and H. Knözinger, Angew. Chem. Int. Ed. 27 (1988) 1127.
[22] K. Asakura, H. Nagahiro, N. Ichikuni and Y. Iwasawa, Appl. Catal. A-Gen. 188 (1999) 313.
[23] A.M. Argo, J.F. Odzak, F.S. Lai and B.C. Gates, Nature 415 (2002) 623.